SCIENCE CHINA
Chemistry

• ARTICLES •

HOT PAPER

May 2015 Vol.58 No.5: 879–884
doi: 10.1007/s11426-014-5315-4

Biosensing strategy based on photocurrent quenching of quantum dots via energy resonance absorption

Guangming Wen, Peng Wang, Wenwen Tu, Jianping Lei & Huangxian Ju*

State Key Laboratory of Analytical Chemistry for Life Science; School of Chemistry and Chemical Engineering, Nanjing University, Nanjing 210093, China

Received July 28, 2014; accepted August 25, 2014; published online March 12, 2015

A new concept of energy resonance absorption for photocurrent quenching was proposed using a system of quantum dots (QDs) and the matched dye. The QDs were used as the photocurrent producer, and the dye had an absorption band overlapped with that of the QDs, which led to the resonance absorption of the excitation energy and thus decreased the photocurrent of QDs. By using porphyrin and fluorscein isothiocyanate isomer I as the resonance absorption dyes, the proposed mechanism was proved by UV-Vis spectra, photoluminescence spectra and photocurrent-to-wavelength response, respectively. The interaction of the absorption-matched dye with biomolecule could be conveniently used to introduce it into the photocurrent quenching system, leading to a simple switch-off biosensing method for detection of the biomolecule. As example, a label-free method was proposed for photoelectrochemical detection of target DNA. This method showed a detection range from 6.0 to 600 nmol/L with a detection limit of 2.5 nmol/L. The result demonstrated that the photocurrent quenching via energy resonance absorption not only contributed to the theoretical study of photoelectrochemistry, but also provided a universal tool for photoelectrochemical biosensing.

energy resonance absorption, photocurrent quenching, photoelelctrochemistry, biosensing, DNA

1 Introduction

Photoelectrochemistry has attracted widespread research interest owing to its significant applications in varieties of fields such as cell fabrication [1–5] and organic synthesis [6,7]. Its advantages including little destructive effect on biological samples [8], separation of the electrical signal from light signal [9,10] and low applied potential [11,12] have led to excellent analytical performance for photoelectronchemical (PEC) detections of proteins [13–15] metal ion [10], DNA [16,17] and small molecules like dopamine [18] and H_2O_2 [19]. In these protocols, the detection signals are usually produced through five ways: (1) use photocurrent producers such as semiconductor nanoparticles [9,20,21] and nanoparticle conjugates [22] as signal tags for signal-on PEC sensing; (2) utilize the sensitizing effect of analyte on photocurrent producer to design PEC sensing methods [11,18,19]; (3) form the trapping sites of produced excitons by the interaction of analytes such as metal ions with the producers to decrease the photocurrent [10]; (4) inhibit the electron emission via the energy transfer from the producer to tag labeled to analyte [23–25]; (5) form some precipitates on photocurrent producer by analyte-related biocatalysis to block the electron transfer for signal-off PEC sensing [14,24]. In the fourth PEC detection protocol, the optical properties of the tag and the distance between the tag and the photocurrent producer must fulfill the conditions for energy transfer [14,23–25], which limits the application of this protocol.

To overcome the limitations occurred in energy transfer-based PEC biosensing, this work proposed a novel concept of energy resonance absorption, which could happen when the absorption band of a dye overlapped the absorption band

*Corresponding author (email: hxju@nju.edu.cn)

of the photocurrent producer. This event decreased the absorption of exciting energy by the producer, thus inhibited electron emission and decreased the photocurrent density. Using quantum dots (QDs) as the photocurrent producer, both fluorscein isothiocyanate isomer I (FITC-I) and Fe(III) tetrakis(1-methyl-4-pyridyl)porphyrin (Fe^{III}TMPyP) were used as the absorption-matched dyes to verify the concept of energy resonance absorption. In comparison with the energy transfer mechanism, the energy resonance absorption possesses less relativity with the distance between the dye and producer. As an example, the specific interaction between tetrakis(4-*N*-methylpyridyl) porphine (H_2TMPyP) and double stranded DNA (ds-DNA) was used for design of a label-free biosensing method. This switch-off photoelectrochemical detection method for target DNA showed good analytical performance. The energy resonance absorption provides a promising universal platform for PEC biosensing.

2 Experimental

2.1 Materials and reagents

Meso-2,3-dimercaptosuccinic acid (DMSA) and cadium chloride ($CdCl_2 \cdot 2.5H_2O$) were purchased from Alfa Aesar China Ltd. (China). Tellurium rod (4 mm in diameter) was purchased from Leshan Kayada Photoelectricity Co. (China). H_2TMPyP and Fe^{III}TMPyP were from Professor Osamu Ikeda at Kanazawa University (Japan) as gifts. FITC-I was purchased from Heowns Co., Ltd. (China). 1-Ethyl-3-(3-dimethylaminopropyl) carbodiimide (EDC) was purchased from Sigma-Aldrich Inc. (USA). Tris(hydroxymethyl)-aminomethane was purchased from Wohong (USA). Target DNA (5′-ATGGGGTCTGTC), amino group labeled probe DNA (5′-GACAGACCCCAT-NH_2-3′), the 4 alkyls modified probe DNA (5′-GACAG-ACCCCAT-$CH_2CH_2CH_2CH_2$-NH_2-3′), 8 alkyls modified probe DNA (5′-GACAGACC-CCAT-$CH_2CH_2CH_2CH_2$-$CH_2CH_2CH_2CH_2$-NH_2-3′), single-base mismatched target (5′-ATGGGTTCTGTC), and double-base mismatched target (5′-ATGTGGTCTTTC) were purchased from Shanghai Sangon Biological Engineering Technology & Services Co., Ltd. (China) and used without further purification. All the other chemicals were of analytical grade. Phosphate buffer saline (PBS, pH 7.2) containing 137 mmol/L NaCl, 2.5 mmol/L $MgCl_2$, and 2 mmol/L KH_2PO_4 was used as electrolyte. All aqueous solutions were prepared using ultra-pure water obtained from a Millipore water purification system (⩾18 MΩ, Milli-Q, Millipore). The indium tin oxide (ITO) membrane covered glass was purchased from Jiangsu Conduc Optics & Electronics Co., Ltd. (China). Prior to use, the ITO glass was cut into 4.5 cm ×0.8 cm slices and successively bathed in 0.5 mol/L NaOH for 10 min, 10% H_2O_2 for 10 min, and acetone for 30 min, and then washed with water and dried in air. The DMSA capped CdTe QDs was synthesized by our previously reported electrolysis method [26].

2.2 Modification of ITO electrode

As the photocurrent producer, 10 μL DMSA capped CdTe QDs was dropped onto ITO electrode and dried at 37 °C to form a stable QDs modified ITO electrode. The QDs-dye modified ITO electrode was prepared by dropping 10 μL of 1 mmol/L dye (H_2TMPyP, Fe^{III}TMPyP, or FITC-I) solution on QDs modified ITO electrode, drying at room temperature, and then washing with 100 μL PBS buffer.

For DNA detection, the DNA probe was linked to the QDs by dropping the mixture of 10 μL 0.5 mg/mL EDC and 10 μL 2.0×10^{-5} mol/L DNA probe on a QDs modified ITO electrode and reaction at room temperature for 30 min. After the electrode was washed with PBS buffer and dried at 37 °C, 10 μL target DNA of different concentrations were dropped on the probe to hybride at 37 °C for 30 min. Afterwards, 10 μL of 3.0 mmol/L H_2TMPyP was added on the layer to react for 20 min. Finally, the ITO was thoroughly washed with water for photocurrent detection.

2.3 Photoelectrochemical response

PEC measurements were performed on an assambled system with a 500 W Xe lamp (CHF-XM-500 W, purchased from Beijing Trusttech Co., Ltd., China), a monochromator (Omni-λ150, purchased from Zolix Instruments Co., Ltd., China), and a CHI660D electrochemical workstation (Shanghai Chenhua Instruments Co., Ltd., China) as the external voltage supplier and the detector of the photocurrent as well. The modified ITO electrode as the working electrode, a platinum wire electrode as the auxiliary electrode and a saturated calomel electrode as the reference electrode were inserted into a quartz PEC cell to form a three-electrode system. 10 mL pH 7.2 PBS was added into the cell as the electrolyte. By setting the monochromator and electrochemical work station for the desired illuminating wavelength and desired external voltage, the photocurrent was recorded upon off-on internals of the illumination.

2.4 Spectroscopic measurements

The UV-Vis spectra were recorded on a UV-3600 UV-Vis-NIR Spectrometer (Shimadzu, Japan). The photoluminescence spectra were recorded on a RF-5301 PC luminescence spectrometer (Shimadzu, Japan). Meanwhile, the circular dichroism (CD) spectra were obtained with a J-810/163-900 Circular Dichroism Spectrometer (JASCO, Japan).

3 Results and discussion

3.1 Photocurrent quenching

DMSA capped CdTe QDs as the photocurrent producer and

H_2TMPyP as an absorption-matched dye were used to verify the new photocurrent quenching mechanism. At the excitation wavelength of 420 nm, the QDs modified on ITO electrode produced excitons on their surface to release electrons into the vacant conduction, which was then accepted by dissolved oxygen to produce a strong cathodic photocurrent (Scheme 1(a)) [10]. Upon the coverage of H_2TMPyP on QDs modified ITO, the photocurrent density (J_p) decreased (Figure 1(a)). The plot of J_p vs the concentration (C) of H_2TMPyP showed a linearity with a regression equation of J_p=–0.41C+0.33 (R^2=0.99, Figure 1(b)). This relationship was different from that for exciton trapping induced photocurrent decreasing [10], implying the different photocurrent quenching mechanism. Considering the facts that the absorbance of H_2TMPyP was positively correlated to its amount coated on ITO and that the linearity was unrelated to the thickness of H_2TMPyP, i.e. the distance between the photocurrent producer and H_2TMPyP, the linear decrease of photocurrent density could be attributed to the absorption of the exciting energy by H_2TMPyP (Scheme 1(b)), which lowered the amount of formed exciton and thus decreased the photocurrent density.

3.2 Energy resonance absorption

The synchronous energy absorption or energy resonance absorption by H_2TMPyP and QDs resulted from the overlapped absorption bands of QDs and H_2TMPyP from 390 to 440 nm (Figure 2(a)). The effect of H_2TMPyP on the excitation intensity of DMSA capped CdTe QDs (Figure 3(a)) and the unmatched emission wavelength of QDs (580 nm, Figure 3(b)) with the absorption band of H_2TMPyP (around 420 nm, Figure 2(a)), which excluded the possibility of energy transfer from excited QDs to H_2TMPyP [27,28] further confirmed the quenching mechanism of energy resonance absorption. In the absence of H_2TMPyP, the excitation spectrum of QDs showed three main excitation bands, ranging from 330 to 374 nm, 376 to 400 nm, and 412 to 463 nm, respectively (Figure 3(a)). Upon the addition of H_2TMPyP, their excitation intensities decreased by 37.6%, 43.8% and 83.3%, respectively. The greater decrease of the excitation band ranging from 412 to 463 nm was attributed to the resonance absorption of H_2TMPyP at its characteristic absorption band.

In the absence of H_2TMPyP the photocurrent density of

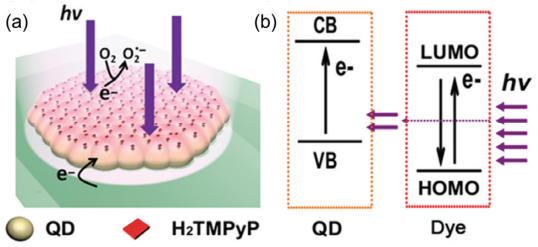

Scheme 1 (a) Schematic illustration of photocurrent generated on QDs-H_2TMPyP modified ITO electrode under irradiation; (b) energy diagram for energy resonance absorption by QDs and H_2TMPyP.

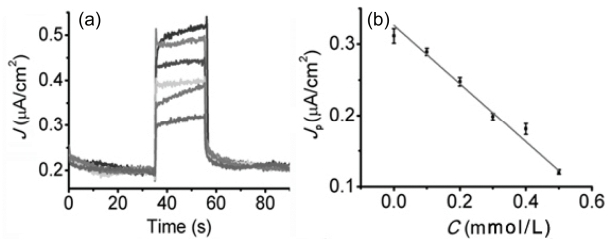

Figure 1 (a) Photocurrent responses of QDs modified ITO electrode covered with 10 μL 0.0, 1.0, 2.0, 3.0, 4.0 and 5.0 mmol/L H_2TMPyP (from top to bottom); (b) plot of photocurrent density vs. the concentration of H_2TMPyP.

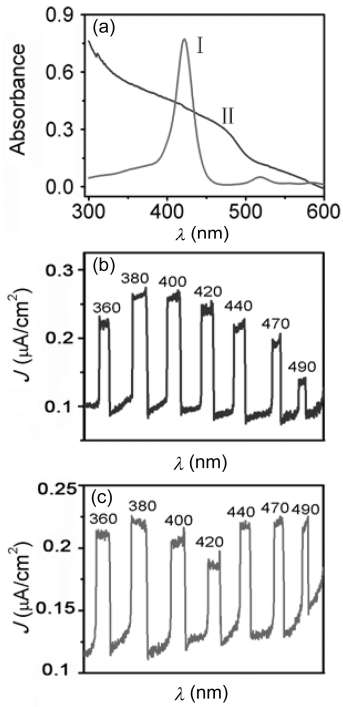

Figure 2 (a) UV-Vis spectra of H_2TMPyP (I) and QDs (II); (b, c) dependence of photocurrent density of QDs (b) and QDs covered with 10 μL 1.0 mmol/L H_2TMPyP (c) on excitation wavelength. The wavelength changes from 360 to 490 nm.

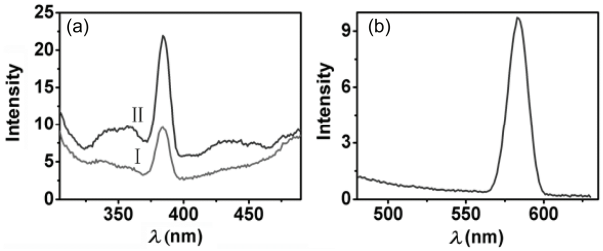

Figure 3 (a) Excitation spectra of as-synthesized DMSA capped CdTe QDs in presence (I) and absence (II) of 1.0 mmol/L H_2TMPyP with an emission wavelength of 580 nm; (b) emission spectrum of as-synthesized DMSA capped CdTe QDs with the excitation wavelength of 380 nm.

QDs increased with the decreasing excitation wavelength and reached the maximum value at 380 nm (Figure 2(b)), as the change of its absorption band (Figure 2(a)). At 360 nm the photocurrent density obviously decreased, though the absorption band continuously increased at shorter wavelength due to the electronic transition between molecular orbitals of QDs instead of that from valence band to conduction band [29,30]. In the presence of H_2TMPyP, the photocurrent density showed different change tendency. It showed a minimum value at 420 nm, smaller than that at 440 nm (Figure 2(c)). The minimum photocurrent density at the characteristic absorption band of H_2TMPyP also confirmed the resonance absorption of H_2TMPyP, which efficiently decreased the excitation energy of QDs.

3.3 Photocurrent quenching by different absorption matched dyes

In order to further verify the photocurrent quenching mechanism of the energy resonance absorption, FITC-I and Fe^{III}TMPyP were used as the absorption-matched dyes, respectively. The main absorption band of FITC-I ranged from 455 to 508 nm with a peak value at 490 nm, and the absorption band of Fe^{III}TMPyP was from 390 to 457 nm with the peak value at 423 nm (Figure 4(a)). These absorption bands overlapped with that of QDs, thus they could produce energy resonance absorption. In the presence of these dyes, the photocurrent density decreased obviously at the overlapped absorption bands (Figure 4(b)). Additionally, similar to H_2TMPyP, the absorption peak of Fe^{III}TMPyP also located in one of the excitation bands (from 412 to 463 nm) of QDs and unmatched with the emission wavelength of QDs for energy transfer. Upon the coverage of Fe^{III}TMPyP on QDs surface, the excitation intensity of QDs decreased by 40%, 26.1%, and 86.6% in the regions of 330 to 374 nm, 376 to 400 nm, and 412 to 463 nm, respectively (Figure 4(c)). The greater decrease of the excitation intensity in the overlapped band resulted from the energy resonance absorption. This mechanism for photocurrent quenching provided a new platform for design of biosensing strategy.

3.4 Application in DNA sensing

By the interaction of the absorption-matched dye with target biomolecules, the proposed photocurrent quenching mechanism could be conveniently used for label-free biosensing. For example, H_2TMPyP could specifically interact with double stranded DNA (ds-DNA) [31–33]. After probe DNA hybridized with target DNA, the circular dichroism (CD) spectrum showed a positive Cotton effect at 270 nm and a negative Cotton effect at 240 nm (Figure 5(a), blue line). In the presence of H_2TMPyP, the CD spectrum showed a new negative signal at 442 nm (Figure 5(a), red line) due to the formation of porphyrin-DNA complex through an intercalation

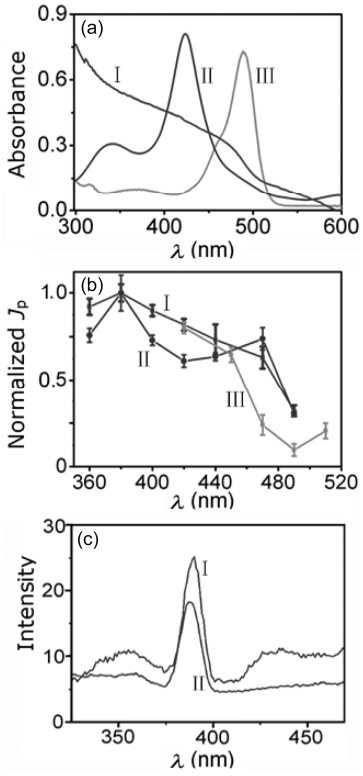

Figure 4 (a) UV-Vis spectra of as-synthesized DMSA capped CdTe QDs (I), 1.0 mmol/L Fe^{III}TMPyP (II), and 1.0 mmol/L FITC-I (III); (b) normalized photocurrent densities at electrodes modified with DMSA capped CdTe QDs (I), QDs and Fe^{III}TMPyP (II), and QDs and FITC-I (III) at different excitation wavelengths; (c) excitation spectra of electrodes modified with DMSA capped CdTe QDs (I), and QDs and Fe^{III}TMPyP (II) at an emission wavelength of 580 nm.

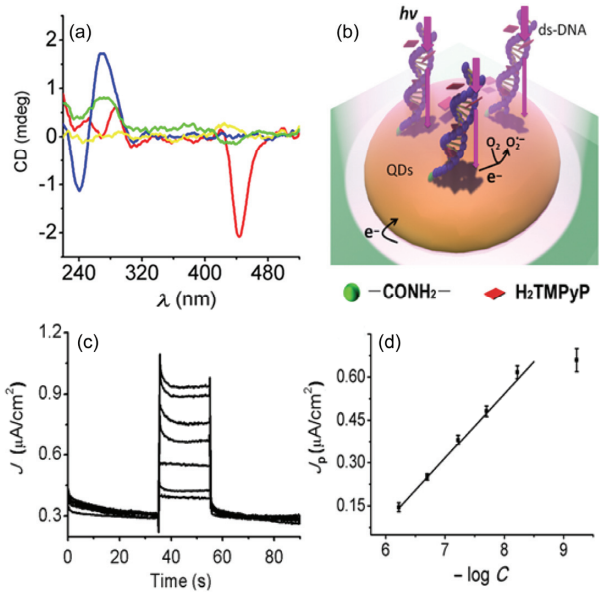

Figure 5 (a) CD spectra of H_2TMPyP (yellow), ds-DNA (blue), ds-DNA in presence of H_2TMPyP (red), and ss-DNA + H_2TMPyP (green); (b) schematic illustration of the DNA sensor; (c) photocurrent responses of the sensor to 0, 0.6, 6.0, 20, 60, 200, and 600 nmol/L (from up to bottom) target DNA with an excitation wavelength of 420 nm; (d) plot of photocurrent density vs. logarithm of target DNA concentration (color online).

interaction [31,32,34], while these signals did not occur for H_2TMPyP alone or the mixture of H_2TMPyP and probe DNA. Thus the DNA sensor could be constructed by simply immobilizing probe DNA functionalized QDs on anITO electrode. After hybridization with target DNA, the formed ds-DNA could capture H_2TMPyP on the sensor surface by the intercalation interaction (Figure 5(b)), which led to the decrease of photocurrent density. With the increasing concentration of target DNA the photocurrent density decreased (Figure 5(c)). The plot of the photocurrent density vs. logarithm value of target DNA concentration showed a good linearity in the concentration range of 6.0 to 600 nmol/L. The detection limit of 2.5 nmol/L was lower than that of $Ru(bpy)_2dppz^{2+}$ labeled PEC method (4.5 nmol/L) [22], competitive PEC method (2.2 μmol/L) [21], and Au nanoparticles based fluorescence resonance energy transfer method (200 nmol/L) [35], showing better analytical performance. In addition, the differentiating ability of the sensor towards the single- and double-base mismatched targets was evaluated. The photocurrent showed the quenched percentage of 42.4%, 11.5% and 3.7% for matched, single- and double-base mismatched strands (Figure 6(a)), showing good selectivity.

Meanwhile, the distance between the producer and dye did not affect the photocurrent quenching or the efficiency of energy resonance absorption (Figure 6(b)). The photocurrent intensities with none-alkyl strands (column 1), 4 alkyls modified strands (column 2) and 8 alkyls modified strands (column 3) as the probe to provide the different distance were almost at the same level. Since the absorption-matched dyes exist widely, this switch-off strategy can easily be extended to the detection of other specific targets.

4 Conclusions

This work proposes a concept of energy resonance absorption for photocurrent quenching. The dyes with an absorption band overlapped with that of photocurrent producer are able to resonantly absorb the excitation energy and thus decrease the photocurrent. Different from the resonance energy transfer, the distance between the photocurrent producer and absorption-matched dye does not affect the efficiency of energy resonance absorption. Moreover, the wide absorption band of QDs as the photo current producers provides extensive opportunities for obtaining the absorption-matched dyes. Thus the proposed mechanism possesses versatility in varieties of fields. As an example of the application, a label-free biosensing method is designed by simply immobilizing probe DNA functionalized QDs on an ITO electrode. The intercalation interaction of H_2TMPyP with ds-DNA leads to good biosensing performance. The photocurrent quenching via energy resonance absorption opens a new avenue for design of photoelectrochemical biosensors and the study of photoelectrochemistry.

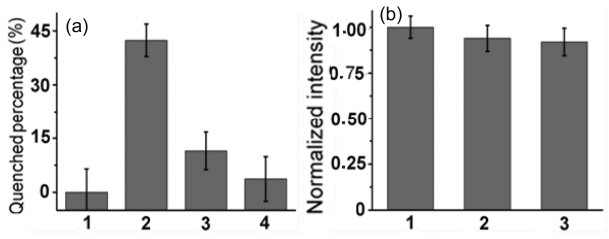

Figure 6 (a) Quenched percentage of the photocurrent intensity in absence of target DNA (column 1), and in presence of matched target (column 2), single- (column 3) and double-base mismatched target (column 4); (b) normalized photocurrent intensity with none-alkyl (column 1), 4 alkyls (column 2) and 8 alkyls modified strands (column 3) as the probe.

This work was financially supported by the National Basic Research Program of China (2010CB732400), and the National Natural Science Foundation of China (21375060, 21135002, 21121091).

1 Gräzel M. Photoelectrochemical cells. *Nature*, 2001, 414: 338–344
2 Christians JA, Fung RCM, Kamat PV. An inorganic hole conductor for organo-lead halide perovskite solar cells. Improved hole conductivity with copper iodide. *J Am Chem Soc*, 2014, 136: 758–764
3 Song QL, Yang HB, Gan Y, Gong C, Li CM. Evidence of harvesting electricity by exciton recombination in an n-n type solar cell. *J Am Chem Soc*, 2010, 132: 4554–4555
4 Peng KQ, Wang X, Li L, Wu XL, Lee ST. High-performance silicon nanohole solar cell. *J Am Chem Soc*, 2010, 132: 6872–6873
5 Guo QJ, Ford GM, Yang WC, Walker BC, Stach EA, Hillhouse HW, Agrawal R. Fabrication of 7.2% efficient CZTSSe solar cells using CZTS nanocrystals. *J Am Chem Soc*, 2010, 132: 17384–17386
6 He MT, Li JB, Tan SB, Wang RZ, Zhang Y. Photodegradable supramolecular hydrogels with fluorescence turn-on reporter for photomodulation of cellular microenvironments. *J Am Chem Soc*, 2013, 135: 18718–18721
7 Jiang H, Cheng YZ, Wang RZ, Zheng MM, Zhang Y, Yu SY. Synthesis of 6-alkylated phenanthridine derivatives using photoredox neutral somophilic isocyanide insertion. *Angew Chem Int Ed*, 2013, 52: 13289–13292
8 Ghezzi D, Antognazza MR, Maschio MD, Lanzarini E, Benfenati F, Lanzani G. A hybrid bioorganic interface for neuronal photoactivation. *Nat Commun*, 2011, 2: 166
9 Yildiz HB, Tel-Vered R, Willner I. CdS nanoparticles/β-cyclodextrin-functionalized electrodes for enhanced photoelectrochemistry. *Angew Chem Int Ed*, 2008, 47: 6629–6633
10 Wang P, Ma XY, Su MQ, Hao Q, Lei JP, Ju HX. Cathode photoelectrochemical sensing of copper(II) based on analyte-induced formation of exciton trapping. *Chem Commun*, 2012, 48: 10216–10218
11 Tu WW, Dong YT, Lei JP, Ju HX. Low-potential photoelectrochemical biosensing using porphyrin-functionalized TiO_2 nanoparticles. *Anal Chem*, 2010, 82: 8711–8716
12 Zhang XR, Li SG, Jin X, Zhang SS. A new photoelectrochemical aptasensor for the detection of thrombin based on functionalized graphene and CdSe nanoparticles multilayers. *Chem Commun*, 2011, 47: 4929–4931
13 Haddour N, Chauvin J, Gondran C, Cosnier S. Photoelectrochemical immunosensor for label-free detection and quantification of anticholera toxin antibody. *J Am Chem Soc*, 2006, 128: 9693–9698
14 Zhao WW, Ma ZY, Yu PP, Dong XY, Xu JJ, Chen HY. Highly sensitive photoelectrochemical immunoassay with enhanced amplifica-

tion using horseradish peroxidase induced biocatalytic precipitation on a CdS quantum dots multilayer electrode. *Anal Chem*, 2012, 84: 917–923
15 Hu CG, Zheng J, Su XY, Wang J, Wu WZ, Hu SS. Ultrasensitive all-carbon photoelectrochemical bioprobes for zeptomole immunosensing of tumor markers by an inexpensive visible laser light. *Anal Chem*, 2013, 85: 10612–10619
16 Yin HS, Sun B, Zhou YL, Wang M, Xu ZN, Fu ZL, Ai SY. A new strategy for methylated DNA detection based on photoelectrochemical immunosensor using Bi_2S_3 nanorods, methyl bonding domain protein and anti-his tag antibody. *Biosens Bioelectron*, 2014, 51: 103–108
17 Wang YH, Ge L, Wang PP, Yan M, Ge SG, Li NQ, Yu JH, Huang JD. Photoelectrochemical lab-on-paper device equipped with a porous Au-paper electrode and fluidic delay-switch for sensitive detection of DNA hybridization. *Lab Chip*, 2013, 13: 3945–3955
18 Hao Q, Wang P, Ma XY, Su MQ, Lei JP, Ju HX. Charge recombination suppression-based photoelectrochemical strategy for detection of dopamine. *Electrochem Commun*, 2012, 21: 39–41
19 Chen D, Zhang H, Li X, Li JH. Biofunctional titania nanotubes for visible-light-activated photoelectrochemical biosensing. *Anal Chem*, 2010, 82: 2253–2261
20 Tel-Vered R, Yehezkeli O, Yildiz HB, Wilner OI, Willner I. Photoelectrochemistry with ordered CdS nanoparticle/Relay or photosensitizer/Relay dyads on DNA scaffolds. *Angew Chem Int Ed*, 2008, 47: 8272–8276
21 Baş D, Boyacı İH. Photoelectrochemical competitive DNA hybridization assay using semiconductor quantum dot conjugated oligonucleotides. *Anal Bioanal Chem*, 2011, 400: 703–707
22 Zhang XR, Zhao YQ, Zhou HR, Qu B. A new strategy for photoelectrochemical DNA biosensor using chemiluminescence reaction as light source. *Biosens Bioelectron*, 2011, 26: 2737–2741
23 Zeng XX, Ma SS, Bao JC, Tu WW, Dai ZH. Using graphene-based plasmonic nanocomposites to quench energy from quantum dots for signal-on photoelectrochemical aptasensing. *Anal Chem*, 2013, 85: 11720–11724
24 Zhang XR, Guo YS, Liu MS, Zhang SS. Photoelectrochemically active species and photoelectrochemical biosensors. *RCS Adv*, 2013, 3: 2846–2857
25 Zhao WW, Wang J, Xu JJ, Chen HY. Energy transfer between CdS quantum dots and Au nanoparticles in photoelectrochemical detection. *Chem Commun*, 2011, 47: 10990–10992
26 Liu X, Cheng LX, Lei JP, Liu H, Ju HX. Formation of surface traps on quantum dots by bidentate chelation and their application in low-potential electrochemiluminescent biosensing. *Chem Eur J*, 2010, 16: 10764–10770
27 Jahan S, Mansoor F, Kanwal S. Polymers effects on synthesis of AuNPs, and Au/Ag nanoalloys: indirectly generated AuNPs and versatile sensing applications including anti-leukemic agent. *Biosens Bioelectron*, 2014, 53: 51–57
28 Medintz IL, Uyeda HT, Goldman ER, Mattoussi H. Quantum dot bioconjugates for imaging, labelling and sensing. *Nat Mater*, 2005, 4: 435–446
29 Platt U, Perner D. Direct measurements of atmospheric CH_2O, HNO_2, O_3, NO_2, and SO_2 by differential optical absorption in the near UV. *J Geophys Res*, 1980, 85: 7453–7458
30 Gergel D, Cederbaum AI. Interaction of nitric oxide with 2-thio-5-nitrobenzoic acid: implications for the determination of free sulphydryl groups by Ellman's reagent. *Arch Biochem Biophys*, 1997, 347: 282–288
31 Balaz M, Napoli MD, Holmes AE, Mammana A, Nakanishi K, Berova N, Purrello R. A cationic zinc porphyrin as a chiroptical probe for Z-DNA. *Angew Chem Int Ed*, 2005, 44: 4006–4009
32 D'Urso A, Mammana A, Balaz M, Holmes AE, Berova N, Lauceri R, Purrello R. Interactions of a tetraanionic porphyrin with DNA: from a Z-DNA sensor to a versatile supramolecular device. *J Am Chem Soc*, 2009, 131: 2046–2047
33 Schwalb NK, Temps F. Base sequence and higher-order structure induce the complex excited-state dynamics in DNA. *Science*, 2008, 322: 243–245
34 Lee S, Jeon SH, Kim BJ, Han SW, Jang HG, Kim SK. Classification of CD and absorption spectra in the Soret band of H_2TMPyP bound to various synthetic polynucleotides. *Biophys Chem*, 2001, 92: 35–45
35 Liu F, Choi JY, Seo TS. Graphene oxide arrays for detecting specific DNA hybridization by fluorescence resonance energy transfer. *Biosens Bioelectron*, 2010, 25: 2361–2365